

**A Raman calibration for the quantification of SO_4^{2-} groups dissolved in
silicate glasses: Application to natural melt inclusions.**

Yann Morizet^{a*}, Emanuela Gennaro^b, Sébastien Jégou^b, Zoltan Zajacz^c, Giada Iacono-
Marziano^b, Michel Pichavant^b, Ida Di Carlo^b, Clément Ferraina^b, Priscille Lesne^b,

^a Laboratoire de Planétologie et Géodynamique de Nantes (LPGN) UMR 6112 CNRS,
Université de Nantes, Nantes Atlantique Universités, 2 rue de la Houssinière, 44322
NANTES (France)

^b Institut des Sciences de la Terre D'Orléans (ISTO) UMR 7327 CNRS, Université d'Orléans
BRGM, Campus Géosciences, 1A rue de la Férolerie, 45071 ORLEANS Cedex 2 (France)

^c Department of Earth Sciences, University of Toronto, 22 Russell St., Toronto, ON M5S 3B1
(Canada)

*Corresponding author: Yann Morizet

Postal address:

Laboratoire de Planétologie et Géodynamique de Nantes (LPG Nantes), UMR-CNRS 6112,
Université de Nantes.

2 rue de la Houssinière, 44322 Nantes Cedex (FRANCE)

phone: +33 (0) 2 5112 5491

fax: +33 (0) 2 5112 5268

*E-mail: yann.morizet@univ-nantes.fr

Abstract:

Sulfur is an important volatile element involved in magmatic systems. Its quantification in silicate glasses relies on state-of-the-art techniques such as electronprobe microanalyses (EPMA) or X-ray absorption spectroscopy but is often complicated by the fact that S dissolved in silicate glasses can adopt several oxidation states (S^{6+} for sulfates or S^{2-} for sulfides). In the present work, we use micro-Raman spectroscopy on a series of silicate glasses to quantify the S content. The database is constituted by 47 silicate glasses of various compositions (natural and synthetic) with S content ranging from 1179 to 13 180 ppm. Most of the investigated glasses have been synthesized at high pressure and high temperature and under fully oxidizing conditions. The obtained Raman spectra are consistent with these fO_2 conditions and only S^{6+} is present and shows a characteristic peak located at $\sim 1000\text{ cm}^{-1}$ corresponding to the symmetric stretch of the sulfate molecular group ($\nu_1\text{ SO}_4^{2-}$). The intensity of the $\nu_1\text{ SO}_4^{2-}$ peak is linearly correlated to the parts per million of S^{6+} determined by EPMA. Using subsequent deconvolution of the Raman spectra, we established an equation using the ratio between the areas of the $\nu_1\text{ SO}_4^{2-}$ peak and the silicate network species (Q^n) in the high frequency region:

$$\text{ppm } S^{6+} = 34371 \frac{A_{SO_4^{2-}}}{A_{Q^n}} \pm 609$$

We tested our calibration on several silicate glasses equilibrated under moderately reducing conditions ($QFM+0.8 \leq fO_2 \leq QFM+1.4$) in which S is dissolved as both SO_4^{2-} and S^{2-} . We also analysed several olivine-hosted melt inclusions collected from Etna and for which the fO_2 and S speciation is unknown. For these samples, the S content estimated by the Raman calibration is systematically lower than the total S measured by EPMA. We combined both methods to estimate the S^{2-} content not accounted for by Raman and derive the S speciation and fO_2

conditions. The derived $f\text{O}_2$ is consistent with the imposed $f\text{O}_2$ for synthesised glasses and with current assumed $f\text{O}_2$ conditions for basaltic melt inclusions from Etna.

Introduction

Sulfur (S) is the most important volatile element in magmatic systems after H_2O and CO_2 (Carroll and Webster 1994; Symonds et al. 1994; Clemente et al. 2004). The S output from volcanic emissions to the atmosphere contributes to the global change in the chemistry of the Earth's atmosphere (Stevenson et al. 2003; Oppenheimer et al. 2011). Even at low concentration, sulfur is partitioned into the fluid phase (Webster et al. 2009; Webster and Botcharnikov 2011; Oppenheimer et al. 2011); hence, playing a major role in the eruptive degassing of many volcanic eruptions (Scaillet et al. 2003). However, high sulfur concentrations can be found in natural melt inclusions from various geological settings (Métrich and Wallace 2008; Vigouroux et al. 2008; Mitchell and Dawson 2012), suggesting S enrichment in the silicate melt at pre-eruptive conditions.

Experimental investigations have provided numerous constraints on how S behaves in silicate melts at magmatic conditions (O'Neill and Mavrogenes 2002; Tsujimura et al. 2004; Scaillet and Pichavant 2005; Jugo et al. 2005, 2010; Lesne et al. 2011). However, the different oxidation state that S can take as a function of $f\text{O}_2$ represents a major difficulty for the understanding of S behaviour in silicate melts. In magmatic systems, S is present dissolved in silicate melt mainly as sulfides (S^{2-}) and sulfates (S^{6+}) (e.g. Fincham and Richardson 1954; Carroll and Rutherford 1988; Métrich and Clocchiatti 1996; O'Neill and Mavrogenes 2002; Moretti and Ottonello 2003; Klimm and Botcharnikov 2010; Métrich and Mandeville 2010). The sulfate (SO_4^{2-}) groups are dissolved in silicate melts when oxidizing conditions are prevailing whereas it is present as sulfide (S^{2-}) species when more reducing conditions are achieved (e.g. Métrich and

Clocchiatti 1996; Jugo et al. 2005; Baker and Moretti 2011). Therefore, S speciation in silicate melt constitutes a good proxy for silicate melt redox state.

The quantification of S in silicate glasses either in experimental charges or in natural magmatic rocks relies mainly on the use of Electron Micro-Probe Analysis (EPMA) technique (e.g. Métrich and Clocchiatti 1996; O'Neill and Mavrogenes 2002; Scaillet and McDonald 2006; Moune et al. 2007, 2009; Morizet et al. 2013a, 2015a) or Secondary Ion Mass Spectrometry (SIMS; e.g. Hauri et al. 2002). The EPMA method has also been used to determine the oxidation state of S speciation in silicate glasses (Carroll and Rutherford 1988; Beermann et al. 2011). However, more advanced analytical techniques are routinely used to discriminate between oxidized (S^{6+}) and reduced (S^{2-}) S species such as X-ray absorption spectroscopy (e.g. Paris et al. 2001; McKeown et al. 2004; Fleet et al. 2005; Wilke et al. 2008; Métrich et al. 2009; Jugo et al. 2010; Stelling et al. 2011; Klimm et al. 2012a,b) and Micro-Raman spectroscopy (Klimm and Botcharnikov 2010; Wilke et al. 2011; Morizet et al. 2013a). Determining S speciation in solid samples using Nuclear Magnetic Resonance also offers great potentialities (Couch et al. 2004; Wilke et al. 2011; Klimm et al. 2012a). In comparison to previously mentioned analytical techniques, micro-Raman spectroscopy is a more accessible analytical technique in laboratories. Furthermore, micro-Raman spectroscopy appears more straightforward as it is rapid (i.e., spectra are acquired within a few minutes) and necessitates only little preparation of the sample.

Sulfur dissolved in silicate network structure as SO_4^{2-} molecular groups exhibits a strong Raman activity at $\sim 1000\text{ cm}^{-1}$ corresponding to the symmetric stretch vibration of the S-O bonds (ν_1 SO_4^{2-} ; McKeown et al. 2001; Tsujimura et al. 2004; Manara et al. 2007; Lenoir et al. 2009; Klimm and Botcharnikov 2010; Morizet et al. 2013a). The position of this peak is dependent on the charge balancing cation and has been shown to vary from 960 to 1060 cm^{-1} in crystalline phases from $PbSO_4$ to $BeSO_4$ (McKeown et al. 2001). In the case of crystalline sulfates,

additional vibrations are also present but in lower intensity (Manara et al. 2007; White 2009) as compared to the $\sim 1000\text{ cm}^{-1}$ peak intensity. The case of S^{2-} in reduced conditions is more complex as the Raman activity is dependent on the silicate glass composition. For instance, in Fe-free H_2O -bearing silicate glasses, S^{2-} species are dissolved in the melt structure as HS^- groups producing a Raman signal at $\sim 2570\text{ cm}^{-1}$ attributed to the symmetric stretch vibration of the H-S bond (Klimm and Botcharnikov 2010; Morizet et al. 2013a). For Fe-bearing natural silicate glasses, S^{2-} species dissolves in silicate melt structure by forming Fe-S complexes. By comparison with sulfide crystalline compounds, Klimm and Botcharnikov (2010) suggested that such dissolution mechanism in silicate melts leads to a peak located at $\sim 400\text{ cm}^{-1}$ (Hope et al. 2001; Mernagh and Trudu 1993; White 2009); however, a reliable quantification of such reduced species is hampered by the strong overlapping of the 400 cm^{-1} peak and the bridging oxygen bending vibration of the silicate network (Mysen et al. 1980; McMillan 1984; Mysen and Frantz 1994; Malfait et al. 2007).

Raman spectroscopy is an analytical technique initially non-quantitative; however, recent progresses have led to the establishment of quantitative calibration of volatiles species dissolved in silicate glasses such as H_2O (Thomas 2000; Zajacz et al. 2005; Mercier et al. 2009; Le Losq et al. 2012) and more recently CO_2 dissolved as carbonate groups (CO_3^{2-} ; Morizet et al. 2013b). For S species, Lenoir et al. (2009) reported a quantitative Raman calibration for SO_4^{2-} dissolved in borosilicate glasses (i.e. with an industrial purpose) for S content up to $\sim 6000\text{ ppm}$. They found that the $\nu_1\text{ SO}_4^{2-}$ intensity at $\sim 1000\text{ cm}^{-1}$ is linearly correlated to the S content (expressed as SO_3) but the calibration factor appears dependent on the glass chemical composition. More recently Klimm et al. (2012a) proposed an equation to determine the S speciation in Fe-free to Fe-poor silicate glasses dissolving S as both SO_4^{2-} and HS^- . This calibration has been established on ~ 15 data point of various silicate glass compositions with S speciation is constrained from XANES data.

In the present work, we establish a calibration using Raman spectroscopy to quantitatively determine the S content dissolved as SO_4^{2-} groups in silicate glasses. We used an extensive database of silicate glasses of various chemical compositions either natural (basaltic to dacitic) or synthetic (Fe-free compositions), with S content from 1179 to 13180 ppm. Silicate glasses used in the calibration were synthesised under oxidizing conditions and S is dissolved as sulfate molecular groups (SO_4^{2-}). We tested the capability of our linear calibration independent of the glass composition to estimate redox conditions, on both experimental glasses and natural melt inclusions. We initially used basaltic glasses synthesised under known moderately reducing conditions to retrieve the $f\text{O}_2$ at which they were equilibrated. We then estimated the $f\text{O}_2$ of natural melt inclusions from Mt. Etna, and compared to previous estimates.

Sample description

Sample set for calibration of SO_4^{2-} content

To establish the present calibration, we analysed a series of silicate glasses synthesised under pressure (up to 0.5 GPa) and equilibrated with different amount of S. The sample dataset is reported in Table 1 along with the major elements chemical composition, and the S content. This dataset is the most extensive compilation considered so far for establishing a calibration of the S content using Raman spectroscopy with 47 data points with a wide range of silicate melt compositions: SiO_2 from 46 to 68 wt.%, Al_2O_3 from 13 to 20 wt.%, FeO^{tot} up to 11 wt.%, CaO from 1.5 to 24 wt.%, MgO up to 11 wt.%, Na_2O up to 8 wt.% and K_2O up to 9 wt.% and S content from 1179 to 13180 ppm. The investigated samples have either Fe-free synthetic or Fe-bearing natural compositions, and are mostly obtained from previous works. For Fe-free synthetic glasses, we analysed samples from Morizet et al. (2013a, 2015a) having composition of Anorthite-Diopside eutectic, and from Zajacz (2015) having various compositions from the

simplest in the CaO-Al₂O₃-SiO₂ system to the more complex in the Na₂O-K₂O-CaO-FeO-MgO-Al₂O₃-SiO₂ system. Investigated natural glass compositions are various. Samples from Jégo and Pichavant (2012) have dacitic compositions with SiO₂ > 67 wt.%. Glass samples from Pichavant et al. (2006), Lesne (2008), Lesne et al. (2011), and Gennaro (2017) have alkali basaltic compositions and were synthesised from natural rock powders collected from different volcanic centres (e.g. Etna, Vesuvius, Stromboli, Mt Pelée and Soufriere St Vincent). Glass samples from Iacono-Marziano et al. (*subm.*) have basaltic-picritic compositions obtained from the minor crystallization of a picritic rock from Noril'sk 1 intrusion (Russia).

All the investigated glasses were synthesised using high pressure apparatuses (either piston-cylinder or Internally Heated Pressure Vessel) and have been equilibrated under oxidizing conditions at more than 1 log unit above the Quartz-Fayalite-Magnetite solid buffer ($fO_2 > QFM+1$, see Table 1). These fO_2 conditions are reported in the considered publications and often represent the intrinsic fO_2 conditions at pressure and temperature in IHPV (Lesne et al. 2011) and piston-cylinder (Morizet et al. 2015a) apparatuses. Zajacz (2015) imposed very oxidizing conditions ($fO_2 > QFM+1.8$) in piston-cylinder experiments by using Re-ReO₂ solid buffer. Pichavant et al. (2006), Gennaro (2017), and Iacono-Marziano et al. (*subm.*) conducted their experiments in IHPV apparatuses, using variable hydrogen partial pressures. The fO_2 was estimated by redox sensor methods (Co-Pd-CoO, Ni-Pd-NiO; Pownceby and O'Neill 1994), from the composition of the solid sensor and the determined H₂O content (see Morizet et al. 2010).

Under the reported oxidizing conditions in Table 1, S is mostly present as SO₄²⁻ species (Nagashima and Katsura 1973; Carroll and Rutherford 1988; Jugo et al. 2005, 2010; Klimm et al. 2012). X-ray absorption spectroscopic data on HAB27, 28 and Ca-3 show only the presence of sulphate species (Pichavant et al. *in review*).

More generally, the considered studies do not report any evidence of reduced sulfur species dissolved in the silicate glasses, except Morizet et al. (2013a), who observed by Raman spectroscopy a small proportion of HS⁻ in sample AD-5-5, and estimated it to represent less than 3% of the total S.

Moderately reduced basaltic glasses

Six basaltic glasses synthesised in IHPV from natural rock powders at 80-200 MPa and 1200°C and under moderately reducing conditions ($0.8 < fO_2 \leq \text{QFM}+1.6$; Gennaro 2017; Iacono-Marziano et al. *subm.*) have been considered (see Table 1). Under the fO_2 conditions estimated for these samples, Jugo et al. (2010) showed that oxidized sulfate species (S⁶⁺ dissolved as SO₄²⁻ molecular groups) and reduced sulfides species (S²⁻ complexed to Fe atoms) coexist in basaltic melt compositions. We therefore used the equation (Eq. 1) of Jugo et al. (2010) to estimate the molar fraction of oxidized sulfur (XS⁶⁺, Table 1) in the six experimental glasses:

$$S^{6+} / \sum S = 1 / (1 + 10^{(2.1 - 2\Delta FMQ)}) \quad \text{Eq. 1}$$

With Eq. 1, we determined XS⁶⁺ at 0.4, 0.6, 0.8 and 0.8 for 27034, 27042, 27031 and 27032 samples, respectively. It should be emphasised that the calculated molar fractions are probably tainted with a large error considering that under those fO_2 conditions the change in S speciation is very fast and any slight variation in fO_2 will induce a strong change in XS⁶⁺ (Jugo et al. 2010; Wilke et al. 2011).

Our calibration was also tested via the analyses of natural basaltic glass inclusions entrapped in olivine crystals collected at Etna volcano from pyroclastic products dated at 4000 years ago (Coltelli et al. 2005; Kamenetsky et al. 2007) and lava flow dated at 10000-15000 years ago (Kamenetsky and Clocchiatti 1996), in which S speciation (and fO_2) are unknown (see Table

1). Therefore, there is an interest as to whether or not it is possible to derive the concentration of S^{2-} , and thus the speciation of S, by calculating the difference between the total S concentration as determined by EPMA and the SO_4^{2-} concentration obtained by Raman spectroscopy. By extension, it would be possible to estimate the fO_2 conditions at which the melt inclusions equilibrated. Data of the glass inclusions are reported in Table 1 and an example of glass inclusions is shown in Figure 1. The inclusions are basaltic in composition and the total S concentration determined by EPMA ranges from 1100 to 2570 ppm (see Appendix Table 1).

Analytical methods

Electronprobe microanalyses for S content

The major element concentrations determined by EPMA are reported in Table 1 and were collected from the scientific publications from which the silicate glasses are issued. Full details on the analytical methods of the major element concentrations along with the associated errors can be found from the subsequent references.

The glass S content was determined for each glass sample from at least 10 analyses. In most studies, analytical conditions were usually 50 to 70 nA beam current, 15kV accelerating voltage and 60s peak counting time on one spectrometer. Jégo and Pichavant (2012) used a 10s counting time on each spectrometer. The error on the S content in Table 1 represents the standard deviation calculated from the replicate analyses. Several standards were used for calibrating the S signal from EPMA. Zajacz (2015) used anhydrite ($CaSO_4$) and barite ($BaSO_4$) crystalline standards. Standards used in Gennaro (2017), Lesne (2008), Lesne et al. (2011), Jégo and Pichavant (2012), Morizet et al. (2013a, 2015a) and Pichavant et al. (2006) are synthetic hydrous dacitic glasses with 750, 1400 and 1900 ppm (Clemente et al., 2004). The reported error on S content from EPMA is on average ± 402 ppm; although several samples exhibit large

error on their determined S content such as the AD-5-5 for which an error of ± 3397 ppm is given by Morizet et al. (2013a).

Micro-Raman spectroscopy

We conducted the micro-Raman analyses on two different spectrometers. For silicate glasses synthesised under oxidizing conditions, we used a Jobin-Yvon LabRam 300 spectrometer equipped with an Innova 300-5W Argon ion laser from Coherent© operating at a wavelength of 514 nm. Natural silicate glass inclusions and silicate glasses synthesised under moderately reducing conditions (Gennaro 2017) were analysed on a Jobin-Yvon LabRam HR800 equipped with a solid-state diode laser operating at 532 nm. The LabRam 300 spectrometer is equipped with a 2400 grooves/mm grating and the spectral resolution is determined to be on the order of 1 cm^{-1} . The LabRam HR800 spectrometer is equipped with a 1800 grooves/mm grating allowing a spectral resolution better than 0.5 cm^{-1} . On both spectrometers, the analyses were performed in confocal mode and the spatial resolution is better than $2\text{ }\mu\text{m}$. On the LabRam 300, a x50 Olympus objective was used for the analyses of the synthesised glasses; on the LabRam HR 800, a x100 Olympus objective was used for the analyses of the melt inclusions. In confocal mode, the depth resolution of the analyses is lower than $5\text{ }\mu\text{m}$ on the LabRam 300 and better than $2\text{ }\mu\text{m}$ on the LabRam HR 800. The backscattered Raman signal was collected in between 200 and 1250 cm^{-1} . Analyses were also conducted in the 2500 cm^{-1} region to check for the possible presence of HS^- groups. The spectral frequency position was calibrated using the emission lines of Ne- and Hg-lamps.

On both spectrometers, the output power was set to between 50 and 125 mW depending on the sample composition. For Fe-bearing silicate glasses, the output power of the laser was kept low in order to avoid sample heating and melting; for synthetic Fe-free samples, an output power of

125 mW could be used without damaging the glass chips. Several spectra were collected on each glass samples. For each spectrum, we performed 5-10 scans on a given sample with an acquisition time of 15 to 60 s on the LabRam 300. Due to the small size of the glass inclusions ($\sim 40\text{ }\mu\text{m}$) as shown in Figure 1, at best two spectra were collected on each inclusion with the LabRam HR 800. For silicate glass inclusions, 5 scans of 10 s were sufficient to obtain a good signal to noise ratio. The use of two different spectrometers and different analytical conditions does not represent a problem. For instance, we provide in the Supplementary material Raman spectra acquired on both spectrometers for a typical sample (IN52). The Raman spectra are almost identical and subsequent treatment of the spectra lead to comparable results in term of S content as determined from the calibration. This is consistent with previous works that have demonstrated that analytical conditions are not influencing subsequent quantitative Raman calibrations (e.g. Le Losq et al. 2012; Morizet et al. 2013b; Di Genova et al. 2015, 2016). This is especially true considering that the calibration of the SO_4^{2-} Raman signal with the aluminosilicate network Raman signal are located in the same frequency range ($800\text{-}1200\text{ cm}^{-1}$); therefore detector sensitivity will be identical for the SO_4^{2-} and the aluminosilicate network Raman signals (Le Losq et al. 2012).

Results:

Spectrum description

Typical spectra are shown in Figure 2 for different samples (see figure and caption for details). A typical Raman spectrum acquired for each glass sample is provided in Supplementary material.

The Raman spectra in Figure 2 consist of two different regions: the Low Frequency (LF) region at $200\text{-}650\text{ cm}^{-1}$ and the High Frequency (HF) region at $800\text{-}1250\text{ cm}^{-1}$. The LF is commonly

assigned to vibration of bridging oxygens in membered-ring configuration (Mysen et al. 1980; McMillan et al. 1982; Seifert et al. 1982; Neuville and Mysen 1996; Pasquarello 2001; Le Losq et al. 2013; Di Genova et al. 2015, 2016). This spectral region is often complicated to apprehend as the nature of the vibrations (stretching or bending) is not clearly known (Le Losq et al. 2013) and is a mixture of several types of vibrations. Due to the complexity of interpreting the vibrations in the LF region, we will not use it for establishing our calibration. The HF region is attributed to the stretching vibration of T-O (T = Si⁴⁺, Al³⁺ mainly) bonds in non-bridging oxygens and T-O-T stretching vibration in fully polymerized tetrahedral unit called Qⁿ species (Mysen et al. 1982; Seifert et al. 1982; Neuville and Mysen 1996; Le Losq et al. 2013, 2014; Di Genova et al. 2015, 2016; Moussallam et al. 2016). The HF vibrational region will be used for establishing our calibration.

The SO₄²⁻ Raman signal is located at ~1000 cm⁻¹ (Figure 2) and attributed to the symmetric stretch (ν_1) of the S-O bonds (Bény et al. 1982; Dubessy et al. 1992; Burke 2001; McKeown et al. 2001; Lenoir et al. 2009; White 2009; Klimm and Botcharnikov 2010; Wilke et al. 2011). In comparison to crystalline sulfate (gypsum or anhydrite for example), the ν_1 SO₄²⁻ peak observed in silicate glasses appears broader suggesting that SO₄²⁻ groups are dissolved within the amorphous structure of the silicate glasses. The broader shape is attributed to a larger distribution in S-O bond length and O-S-O angles in the SO₄²⁻ groups as compared to the crystalline equivalent. From Figure 2 and peak maximum determination, the apparent SO₄²⁻ peak position varies from 990 to 1005 cm⁻¹. This variation in ν_1 SO₄²⁻ has also been mentioned by McKeown et al. (2001) and is due to the nature of the surrounding charge compensating cation for the negative charges of the SO₄²⁻ molecular group. It is clearly seen that as S content increases there is an increase in the relative intensity of the ~1000 cm⁻¹ peak suggesting that the Raman signal intensity is proportional to the concentration of active molecular S-O bonds.

In Figure 2E and F, we show the spectra for samples for which a mixture of SO_4^{2-} and S^{2-} species is expected. The peak for SO_4^{2-} groups is visible at $\sim 1000 \text{ cm}^{-1}$ (less clear for synthesised basalt due to the strong overlapping between the peaks) and we observe a prominent broad peak located at $\sim 400 \text{ cm}^{-1}$. As stated earlier, based on the Raman spectra of sulphide crystalline compounds (pyrite, marcasite; see White 2009), Klimm and Botcharnikov (2010) proposed an assignment of this peak to S^{2-} species complexed with Fe cations. The location of this peak in the LF region 1) on the shoulder of the silicate network line shape and 2) in a region where the baseline is strongly non-linear makes it difficult to investigate (i.e. peak area determination).

Spectrum deconvolution

We used a protocol similar to Morizet et al. (2013b) for deconvolution of the HF region and determination of the $\nu_1 \text{SO}_4^{2-}$ peak area. The first step involves the background subtraction from the Raman raw spectrum. Currently, there is no physical systematic for this step and the subtraction of the background is realised by subtracting a non-linear (third-order polynomial function or cubic spline function) baseline (Di Muro et al. 2006; Behrens et al. 2006; Le Losq et al. 2012; Morizet et al. 2013b; Rossano and Mysen 2013). The baseline is anchored in regions which have no bands. Those regions are indicated by the arrows in Figure 2B and are located at Raman shift below 300 cm^{-1} , around 800 cm^{-1} and above 1200 cm^{-1} , their exact position being strongly dependant on the glass composition. For instance, the beginning of the no band high frequency region is 1200 cm^{-1} for Anorthite-Diopside eutectic, and basaltic – alkali and basaltic glasses (Figures 2A, D, E, F) whereas it is 1250 cm^{-1} for dacitic glasses (Figure 2C), due to the difference in the distribution of the silicate network units as a function of the chemical composition (e.g. McMillan 1984; Mysen 1999; Moussallam et al. 2016). Furthermore, in Figure 2E, we observe that the region of no band at 800 cm^{-1} for the basaltic glasses synthesised under moderately reducing conditions from Gennaro (2017) is at 620 cm^{-1} . Those spectra

exhibit a relatively flat background (acquisition on the LabRam HR 800) but the signature between 600 and 800 cm^{-1} had to be included in the deconvolution procedure.

After the background subtraction, the HF envelop is simulated with five individual Gaussian peaks: one peak corresponding to the ν_1 SO_4^{2-} peak and four peaks corresponding to the stretching vibrations of the silicate network units (Q^n). The most difficult step is the initial parametrization of the Gaussian lines. We placed the ν_1 SO_4^{2-} peak at 1000 cm^{-1} and with a Full Width at Half Maximum (FWHM) of 25 cm^{-1} . This width value has been chosen in the light of the SO_4^{2-} group dissolution mechanisms. Recent works suggest that SO_4^{2-} dissolves in the silicate melt structure either by scavenging non-bridging oxygen (Morizet et al. 2013a, 2015b) or possibly in a similar way to CO_3^{2-} groups by forming free $\text{M}^{n+} \cdot \text{SO}_4^{2-}$ clusters (Brooker et al. 2001b; Machacek et al. 2010; Morizet et al. 2015b; Moussallam et al. 2016) where M^{n+} is a charge balancing cation of different nature (e.g. Ca^{2+} or Mg^{2+}). In both cases, the SO_4^{2-} molecule geometry is only weakly perturbed by the surrounding silicate network; therefore the S-O bond length and O-S-O bond angles have a limited distribution.

The four Gaussian lines for the Q^n units have been initially set at 60-65 cm^{-1} for the FWHM. The geometry of the different Q^n units is more affected by the surrounding cations and the interconnectivity in between the Q^n units and the distribution in T-O length and O-T-O angles is larger. We placed the four Gaussian lines at 1100, 1050, 950 and 875 cm^{-1} as an initial guess (Rossano and Mysen 2013). Those line positions are consistent with the limited range of investigated composition ($46 < \text{SiO}_2 < 68$ wt.%). For instance, for silica-undersaturated melt compositions, the line at 1100 cm^{-1} attributed to Q^4 units will not appear (Moussallam et al. 2016).

Initially, all the peak position and FWHM are kept fixed in order to optimise the peaks area. Because, we consider that sulfur behave as a dilute compound in a solvent, we firstly optimize

the peak position and FWHM of the Q^n units. Only after this optimization, the peak position and FWHM of the $\nu_1 \text{SO}_4^{2-}$ are left free to evolve until optimization. These two steps are repeated several times in order to obtain the best chi-square (χ^2) which is a parameter reflecting the deconvolution efficiency and the robustness of the deconvolution. It should be pointed out that this method provides only one possible solution which might represent only a local minimum. Two additional Gaussian lines were necessary for basaltic glasses synthesised under moderately reducing conditions (Gennaro 2017). These lines could be assigned to vibrations of tetrahedra in a membered ring configuration (Seifert et al. 1982; Pasquarello et al. 1998). Optimization of these lines was conducted in a similar way to the others. The results are reported in the Supplementary material 1. Those peak positions are ~ 795 and 720 cm^{-1} and FWHM $\sim 90 \text{ cm}^{-1}$. It should be pointed out that those two additional Gaussian lines were not included in the calculation of the $A \text{SO}_4^{2-} / A \text{HF}$ ratio and only the Gaussian lines corresponding to Q^n units have been taken into consideration.

In Figure 3, we show several deconvolution results for different compositions, from low S content in C7D (Figure 3C) to high S content in 263b (Figure 3B), and for basaltic glasses synthesised under reducing conditions (Figure 3E) and basaltic glass inclusions (Figure 3F). The spectra are reported along with the simulated envelop and Gaussian lines. The deconvolution results are provided in the Supplementary material 1; derived peak position and FWHM are listed in Table 2. As shown in Table 2, the $\nu_1 \text{SO}_4^{2-}$ peak position varies from 987.9 to 1008.9 cm^{-1} with an average derived position at 999.7 cm^{-1} ; $\nu_1 \text{SO}_4^{2-}$ FWHM varies from 23.2 to 51.8 cm^{-1} with an average value at 34.1 cm^{-1} . The error on $\nu_1 \text{SO}_4^{2-}$ peak position and FWHM is on the order of $\pm 0.5 \text{ cm}^{-1}$ as reported by the deconvolution software package (Origin 7.5[®]). The peak location variability is probably due to the varying charge compensating cation around the SO_4^{2-} group as inferred by McKeown et al. (2001) for S-bearing borosilicate glasses and by White (2009) for crystalline sulphates. However, because investigated glass samples

were synthesised under different pressure and temperature conditions, we cannot rule out any effect of the intensive conditions on the ν_1 SO_4^{2-} peak position and FWHM as witnessed for the ν_1 CO_3^{2-} peak position (Morizet et al. 2013b).

From Figure 3, we observe that the intensity of the 1000 cm^{-1} peak obtained from the spectrum deconvolution increases with the increase in the S content measured by EPMA. There is a strong overlapping between the lines that makes the determination of the part per million of S dissolved as SO_4^{2-} difficult in low-S silicate glasses. Although SO_4^{2-} appears to have a strong Raman activity for the symmetric stretch of the S-O bonds due to the high symmetry of the SO_4^{2-} molecular group (T_d point group), obtaining a reliable quantitative deconvolution at S concentrations below 1000 ppm S is unlikely.

Discussion

Calibration for SO_4^{2-} groups dissolved in silicate glasses

For the calibration we used only the glasses in which S is dissolved in the oxidized form. We therefore selected only samples with $\text{XS}^{6+}=1$ (Appendix Table 1) and by checking that they presented no peaks at ~ 400 and $\sim 2570\text{ cm}^{-1}$ in their Raman spectrum. In Figure 3, next to each spectrum, we indicate the ratio $A_{\text{SO}_4^{2-}} / A_{\text{HF}}$ calculated from the area of the ν_1 SO_4^{2-} peak and the total area of the silicate network units in the HF region and derived from the performed deconvolutions (reported in Table 1). The error reported on the ratio corresponds to the standard deviation obtained from the replicated deconvolution on the obtained Raman spectra for a given glass sample. The entire set of results can be found in the Supplementary material 1.

As shown in Figure 4, the ratio $A_{\text{SO}_4^{2-}} / A_{\text{HF}}$ is linearly correlated with the S content determined by EPMA up to 13180 ppm S. Furthermore, the linear trend appears independent

of the glass composition for the range of chemical composition investigated here. It is not surprising to find linear correlation independent of the glass composition. Linear correlation of the Raman vibrational intensity as a function of the concentration of a molecule has been previously shown for CO₂ dissolved as CO₃²⁻ groups (Morizet et al. 2013b) and also for H₂O dissolved in silicate glasses (Le Losq et al. 2012). We fitted a linear function through the data points with the hypothesis that at 0 ppm S the ratio A SO₄²⁻ / A HF = 0. By inversion of the equation provided in Figure 4, the determination of the S content dissolved as SO₄²⁻ groups in silicate glasses is achieved with Eq. 2:

$$ppm S^{6+} = 34371 \frac{A SO_4^{2-}}{A Q^n} \pm 609 \quad \text{Eq. 2}$$

In Eq. 2, the S content is expressed as ppm S⁶⁺ which corresponds to the valence of the S within the SO₄²⁻ group. In Eq. 2, the error on the slope parameter is ±609 ppm based on 47 data points. The sources of error on the determination of the S content by Raman spectroscopy is due to the quality of the spectral deconvolution which is affected by the strong overlapping of the different Gaussian lines of the Qⁿ units and the SO₄²⁻. The average standard deviation is higher than the average one obtained by EPMA ±402 ppm for the 47 experimental data points; but similar to the highest ones (500-1000 ppm; Table 1). The Raman method could therefore represent an alternative to EPMA, although sensibly less accurate, to characterize oxidized glasses with dissolved S contents >1000 ppm.

Determining S speciation and *f*O₂ conditions in natural melt inclusions

We also tested the applicability of the Raman method to determine S speciation (and *f*O₂ conditions from it) in moderately oxidized glasses and natural glass inclusions, starting from the EPMA of the total dissolved S. We employed basaltic glasses synthesised at *f*O₂ conditions

between QFM+0.8 and QFM+1.6 (Gennaro 2017; Iacono-Marziano et al. *subm.*) to test the use of our calibration to estimate the fO_2 . As inferred from Figure 2 and considering the fO_2 conditions, the sulfur speciation in these samples is a combination of oxidized S species (S^{6+}) and reduced S species (S^{2-}).

In Figure 5, we report the ppm S^{6+} calculated from our Raman calibration as a function of ppm S determined by EPMA for natural basaltic glass inclusions and experimental basaltic glasses (Gennaro 2017; Iacono-Marziano et al. *subm.*). We observe that the determined ppm S^{6+} from Raman is lower than the 1:1 line, despite the large error on the derived ppm S^{6+} from Raman spectroscopy. This probably reflects the presence of an unaccounted quantity of sulfur represented by the reduced sulfide S^{2-} complexed to Fe atoms (peak at 400 cm^{-1} systematically observed in these samples). The amount of reduced S cannot be assessed directly by Raman spectroscopy, but can be calculated as the difference between the total S measured by EPMA and the S^{6+} estimated using our calibration. We then used the equation of Jugo et al. (2010), to estimate the fO_2 of each glass sample from the molar fraction of S^{6+} (XS^{6+}). We compared the fO_2 obtained by this method with those estimated by the redox sensor method for the basaltic glasses synthesised at fO_2 between QFM+0.8 and QFM+1.6. We followed the same approach for natural melt inclusions from Mt. Etna and estimated fO_2 conditions between QFM+1.1 and QFM+1.5, in agreement with previous work suggesting redox conditions between QFM+0.7 and QFM+1 (Metrich and Clocchiatti 1996), or even more oxidizing (QFM+1.4), for basaltic inclusions hosted in olivine crystals from 2001 lava flow with S mainly present as S^{6+} species (Metrich et al. 2009).

We reported in Figure 5, the evolution lines of the ppm S^{6+} as a function of total ppm S for constant fO_2 (QFM+1, +1.5 and +3) as determined from the equation of Jugo et al. (2010). The line for QFM+3 represents the most oxidized conditions and all S is present as S^{6+} species. Considering the large error obtained from the Raman method (± 609 ppm), a reliable estimate

of the $f\text{O}_2$ would only be obtained for samples having high S content (<2000 ppm). At such a high S content, the Raman method combined with EPMA analyses can provide an estimate of the $f\text{O}_2$ at ± 0.5 log unit for $f\text{O}_2$ below QFM+1.5.

Implications: determining redox conditions in silicate melt inclusions

The major implication of the present results and methodology is the potential determination of redox conditions in S-bearing silicate melt inclusions. Although, the proposed method is accompanied by a large error; it should be emphasized that the determination of natural magmas redox conditions has always been challenging, especially in presence of sulfur that exhibits a non-linear evolution of its speciation as a function of redox conditions (e.g., Métrich et al. 2009; Baker and Moretti 2011; Wilke et al. 2011). This determination is further complicated by the usually small size of natural silicate melt inclusions, which require micrometer-scale analytical techniques and substantial sample preparation. Micro-Raman spectroscopy allows punctual μm scale analyses, ideal for concentration profile construction; and requires limited sample preparation. As pointed out in the discussion, the combination of EPMA and micro-Raman spectroscopy will allow the determination of the $f\text{O}_2$ conditions with an accuracy of ± 0.5 log unit and for melt inclusions having more than 2000 ppm in total S content. Although, these prerequisites prohibit the determination of the redox conditions for natural systems having low S content, we propose the first straightforward method (combination EPMA and micro-Raman spectroscopy) to determine S content and speciation and by extension redox conditions. Such an approach could be used in S-bearing experimental studies but also in some particular natural systems. As an example, we consider that the proposed method could be applied to the melts generated in the subduction geological setting of Central America. Recent works showed that melt inclusions collected from Central America volcanoes have high S content above 2000 ppm and to more than 4000 ppm S (e.g., Wade et al. 2006; Benjamin et al. 2007; Sadofsky et al. 2008) and for which the redox conditions have never been clearly investigated. Additionally,

recent investigations of the volatile pre-eruptive content in East African Rift silica undersaturated volcanic rocks exhibits extremely high S content up to 1 wt% (Mitchell 2009; Mitchell and Dawson 2012). The present method is totally designated to the determination of the redox condition in this particular setting showing high S content and for which the redox conditions are virtually unknown.

References cited:

Baker, D.R., and Moretti, R. (2011) Modeling the solubility of sulfur in magmas: a 50-year old geochemical challenge. In: Behrens, H., Webster, J.D. (Eds.), *Sulfur in Magmas and Melts: Its Importance for Natural and Technical Processes*. Washington, Mineralogical Society of America, Geochemical Society, *Reviews in Mineralogy and Geochemistry*, 73, 167–213.

Beermann O., Botcharnikov R.E., Holtz F., Diedrich O., and Nowak M. (2011) Temperature dependence of sulphide and sulphate solubility in olivine-saturated basaltic magmas. *Geochimica and Cosmochimica Acta*, 75, 7612-7631.

Behrens, H., Roux, J., Neuville, D.R., and Siemann, M. (2006) Quantification of dissolved H₂O in silicate glasses using confocal microRaman spectroscopy. *Chemical Geology*, 229, 96–112.

Bény, C., Guilhaumou, N., and Touray, J.C. (1982) Native-sulfur-bearing fluid inclusions in the CO₂–H₂S–H₂O–S-system — micro-thermometry and Raman micro-probe (mole) analysis — thermochemical interpretations. *Chemical Geology*, 37, 113–127.

Brooker, R.A., Kohn, S.C., Holloway, J.R., and McMillan, P.F. (2001b) Structural controls on the solubility of CO₂ in silicate melts. Part II: IR characteristics of carbonate groups in silicate glasses. *Chemical Geology*, 174, 241–254.

Burke, E.A.J. (2001) Raman microspectrometry of fluid inclusions. *Lithos*, 55, 139–158.

Carroll, M.R., and Rutherford, M.J. (1988) Sulfur speciation in hydrous experimental glasses of varying oxidation state: results from measured wavelength shifts of sulfur X-rays. *American Mineralogist*, 73, 845–849.

Carroll, M.R., and Webster, J.D. (1994) Solubilities of sulfur, noble gases, nitrogen, chlorine, and fluorine in magmas. In: Holloway, J.R., Carroll, M.R. (Eds.), *Volatiles in Magmas*. Washington, Mineralogical Society of America, Geochemical Society, *Reviews in Mineralogy*, 30, 231–280.

Clemente, B., Scaillet, B., and Pichavant, M. (2004) The solubility of sulfur in hydrous rhyolitic melts. *Journal of Petrology*, 45, 2171–2196.

Coltelli, M., Del Carlo, P., Pompilio, M., and Vezzoli, L. (2005) Explosive eruptions of a picrite: The 3930 BP subplinian eruption of Etna volcano (Italy). *Geophysical Research Letter* 32, L23307, doi:10.1029/2005GL024271.

Couch, S., Howes, A.P., Kohn, S.C., and Smith, M.E. (2004) S-33 solid state NMR of sulphur speciation in silicate glasses. *Solid State Nuclear Magnetic Resonance*, 26, 203–208.

Di Genova D., Morgavi D., Hess K.-U., Neuville D.R., Borovkov N., Perugini D., and Dingwell D.B. (2015) Approximate chemical analysis of volcanic glasses using Raman spectroscopy. *Journal of Raman Spectroscopy*, 46, 1235-1244.

Di Genova D., Kolzenburg S., Vona A., Chevrel M.O., Hess K.-U., Neuville D.R., Ertel-Ingrisch W., Romano C., and Dingwell D.B. (2016) Raman spectra of martian glass analogues: A tool to approximate their chemical composition. *Journal of Geophysical Research Planets*, 121, 740-752.

Di Muro, A., Villemant, B., Montagnac, G., Scaillet, B., and Reynard, B. (2006) Determination of water content and speciation in natural silicic glasses by confocal Raman spectrometry. *Geochimica and Cosmochimica Acta*, 70, 2878–2884.

Dubessy, J., Boiron, M.-C., Moissette, A., Monnin, C., and Sretenskaya, N. (1992) Determinations of water, hydrates and pH in fluid inclusions by micro-Raman spectrometry. *European Journal of Mineralogy*, 4, 885-894.

Fincham, C.J.B., and Richardson, F.D. (1954) The behavior of sulfur in silicate and aluminate melts. *Proc. R. Soc. Lond. A*, 223, 40–62.

Fleet, M.E., Liu, X.Y., Harmer, S.L., and King, P.L. (2005) Sulfur K-edge xanes spectroscopy: chemical state and content of sulfur in silicate glasses. *The Canadian Mineralogist*, 43, 1605–1618.

Gennaro, E. (2016) Sulfur behavior and redox conditions in Etnean hydrous basalts inferred from melt inclusions and experimental glasses. Ph.D. thesis, Università degli Studi di Palermo, pp. 155.

Hauri, E., Wang, J., Dixon, J.E., King, P.L., Mandeville, C., and Newman, S. (2002) SIMS analysis of volatiles in silicate glasses 1. Calibration, matrix effects and comparisons with FTIR. *Chemical Geology*, 183, 99-114.

Hope, G.A., Woods, R., and Munce, C.G. (2001) Raman microprobe mineral identification. *Mineral Engineering*, 14, 1565-1577.

Iacono-Marziano, G., Ferraina, C., Gaillard, F., Di Carlo, I., and Arndt, N. (2017) Assimilation of sulfate and carbonaceous rocks: experimental study, thermodynamic modeling and application to the Noril'sk-Talnakh region (Russia). *Ore Geology Reviews*, in press.

Jégo, S., and Pichavant, M. (2012) Gold solubility in arc magmas: Experimental determination of the effect of sulfur at 1000°C and 0.4 GPa. *Geochimica and Cosmochimica Acta*, 84, 560-592.

Jugo, P.J., Luth, R.W., and Richards, J.P. (2005a) An experimental study of the sulfur content in basaltic melts saturated with immiscible sulfide or sulfate liquids at 1300 °C and 1.0 GPa. *Journal of Petrology*, 46, 783–798.

Jugo, P.J., Wilke, M., and Botcharnikov, R.E. (2010) Sulfur K-edge XANES analysis of natural and synthetic basaltic glasses: Implications for S speciation and S content as function of oxygen fugacity. *Geochimica et Cosmochimica Acta*, 74, 5926–5938.

Kamenetsky, V., and Clocchiatti, R. (1996) Primitive magmatism of Mt. Etna: Insights from mineralogy and melt inclusions. *Earth Planetary Science Letters*, 142, 553-572.

Kamenetsky, V.S., Pompilio, M., Métrich, N., Sobolev, A.V., Kuzmin, D.V., and Thomas, R. (2007) Arrival of extremely volatile-rich high-Mg magmas changes explosivity of Mount Etna. *Geology*, 35, 255-258.

Klimm, K., and Botcharnikov, R.E. (2010) The determination of sulfate and sulfide species in hydrous silicate glasses using Raman spectroscopy. *American Mineralogist*, 95, 1574–1579.

Klimm, K., Kohn, S.C., O'Dell, L.A., Botcharnikov, R.E., and Smith, M.E. (2012a) The dissolution mechanism of sulphur in hydrous silicate melts. I: assessment of analytical techniques in determining the sulphur speciation in iron-free to iron-poor glasses. *Chemical Geology*, 322-323, 237–249.

Klimm, K., Kohn, S.C., and Botcharnikov, R.E. (2012b) The dissolution mechanism of sulphur in hydrous silicate melts. II: Solubility and speciation of sulphur in hydrous silicate melts as a function of fO_2 . *Chemical Geology*, 322-323, 250-267.

Le Losq, C., Neuville, D., Moretti, R., and Roux, J. (2012): Determination of water content in silicate glasses using Raman spectrometry: implications for the study of explosive volcanism. *American Mineralogist*, 97, 779–790.

Le Losq, C., Moretti, R., Neuville, D.R. (2013) Speciation and amphoteric behaviour of water in aluminosilicate melts and glasses: high-temperature Raman spectroscopy and reaction equilibria. *European Journal of Mineralogy*, 25, 777-790.

Le Losq, C., Neuville, D.R., Florian, P., Henderson, G.S., and Massiot, D. (2014) The role of Al^{3+} on rheology and structural changes in sodium silicate and aluminosilicate glasses and melts. *Geochimica and Cosmochimica Acta*, 126, 495-517.

Lenoir, M., Grandjean, A., Poissonnet, S., and Neuville, D.R. (2009) Quantitation of sulfate solubility in borosilicate glasses using Raman spectroscopy. *Journal of Non-Crystalline Solids*, 355, 1468–1473.

Lesne, P. (2008) Etude expérimentale de la solubilité des volatils C-H-O-S dans les basaltes alcalins italiens. Simulations numériques du dégazage chimique : application à l'Etna. Ph.D Thesis, 236 p.

Lesne, P., Kohn, S.C., Blundy, J., Witham, F., Botcharnikov, R.E., and Behrens, H. (2011) Experimental simulation of closed-system degassing in the system basalt- H_2O - CO_2 -S-Cl. *Journal of Petrology*, 52, 1737–1762.

Machacek, J., Gedeon, O., Liska, M., and Marhoul, F. (2010) Molecular simulations of silicate melts doped with sulphur and nitrogen. *Journal of Non-Crystalline Solids*, 356, 2458-2464.

Manara, D., Grandjean, A., Pinet, O., Dussossoy, J.L., and Neuville, D.R. (2007) Sulfur behavior in silicate glasses and melts: Implications for sulfate incorporation in nuclear waste glasses as a function of alkali cation and V_2O_5 content. *Journal of Non-Crystalline Solids*, 353, 12-23.

McKeown, D.A., Muller, I.S., Gan, H., Pegg, I.L., and Kendziora, C.A. (2001) Raman studies of sulfur in borosilicate waste glasses: sulfate environments. *Journal of Non-Crystalline Solids*, 288, 191–199.

McKeown, D.A., Muller, I.S., Gan, H., Pegg, I.L., and Stolte, W.C. (2004) Determination of sulfur environments in borosilicate waste glasses using X-ray absorption near-edge spectroscopy. *Journal of Non-Crystalline Solids*, 333, 74–84.

McMillan, P.F., Piriou, B., and Navrotsky, A. (1982) A Raman spectroscopic study of glasses along the joins silica-calcium aluminate, silica-sodium aluminate, and silica-potassium aluminate. *Geochimica et Cosmochimica Acta*, 46, 2021–2037.

McMillan, P. (1984) Structural studies of silicate glasses and melts—applications and limitations of Raman spectroscopy. *American Mineralogist*, 69, 622–644.

Mercier, M., Di Muro, A., Giordano, D., Métrich, N., Lesne, P., Pichavant, M., Scaillet, B., and Clocchiatti, R. (2009) Influence of glass polymerisation and oxidation on micro-Raman water analysis in alumino-silicate glasses. *Geochimica et Cosmochimica Acta*, 73, 197–217.

Mernagh, T.P., and Trudu, A.G. (1993) A laser Raman microprobe study of some geologically important sulphide minerals. *Chemical Geology*, 103, 113-127.

Métrich, N., and Clocchiatti, R. (1996) Sulfur abundance and its speciation in oxidized alkaline melts. *Geochimica and Cosmochimica Acta*, 60, 4151–4160.

Métrich, N., and Wallace, P.J. (2008) Volatile abundances in basaltic magmas and their degassing paths tracked by melt inclusions. In: Putirka, K.D., Tepley III, F.J. (Eds.). *Minerals, Inclusions and Volcanic Processes*. Washington, Mineralogical Society of America, Geochemical Society, *Reviews in Mineralogy and Geochemistry*, 69, 363–402.

Métrich, N., and Mandeville, C.W. (2010) Sulfur in magmas. *Elements*, 6, 81-86.

Métrich, N., Berry, A.J., O'Neill, H.S.C., and Susini, J. (2009) The oxidation state of sulfur in synthetic and natural glasses determined by X-ray absorption spectroscopy. *Geochimica et Cosmochimica Acta*, 73, 2382–2399.

Mitchell, R.H., and Dawson, J.B. (2012) Carbonate–silicate immiscibility and extremely peralkaline silicate glasses from Nasira cone and recent eruptions at Oldoinyo Lengai Volcano, Tanzania. *Lithos*, 152, 40-46.

Moretti, R., and Ottonello, G. (2003) Polymerization and disproportionation of iron and sulfur in silicate melts: insights from an optical basicity-based approach. *Journal of Non-Crystalline Solids*, 323, 111-119.

Morizet, Y., Paris, M., Gaillard, F., and Scaillet, B. (2010) C-O-H fluid solubility in haplobasalt under reducing conditions: An experimental study. *Chemical Geology*, 279, 1–16.

Morizet, Y., Paris, M., Di Carlo, I., and Scaillet, B. (2013a) Effect of sulfur on the structure of silicate melts under oxidising conditions. *Chemical Geology*, 358, 131–147.

Morizet, Y., Brooker, R.A., Iacono-Marziano, G. and Kjarsgaard, B. (2013b) Quantification of CO₂ dissolved in silicate glasses of various compositions with micro-Raman spectroscopy. *American Mineralogist*, 98, 1788–1802.

Morizet, Y., Ory, S., Di Carlo, I., Scaillet, B., and Echegut, P. (2015a) The effect of sulphur on the glass transition temperature in anorthite-diopside eutectic glasses. *Chemical Geology*, 416, 11-18.

Morizet, Y., Vuilleumier, R., and Paris, M. (2015b) A NMR and molecular dynamics study of CO₂-bearing basaltic melts and glasses. *Chemical Geology*, 418, 89-103.

Moune, S., Sigmarsson, O., Thordarson, T., and Gauthier, P.J. (2007) Volatile evolution in the magmatic system of Hekla volcano, Iceland. *Earth Planetary Science Letters*, 255, 373–389.

Moune, S., Holtz, F., and Botcharnikov, R.E. (2009) Sulphur solubility in andesitic to basaltic melts: implications for Hekla volcano. *Contributions to Mineralogy and Petrology*, 157, 691–707.

Moussallam, Y., Florian, P., Corradini, D., Morizet, Y., Sator, N., Vuilleumier, R., Guillot, B., Iacono-Marziano, G., Schmidt, B.C., and Gaillard, F. (2016) The molecular structure of melts along the carbonatite–kimberlite–basalt compositional joint: CO₂ and polymerization. *Earth Planetary Science Letters*, 434, 129-140.

Mysen, B.O., and Frantz, J.D. (1994) Structure of haplobasaltic liquids at magmatic temperatures: In-situ, high-temperature study of melts on the join Na₂Si₂O₅-Na₂(NaAl)₂O₅. *Geochimica et Cosmochimica Acta*, 58, 1711–1733.

Mysen, B.O. (1999) Structure and properties of magmatic liquids: From haplobasalt to haploandesite. *Geochimica et Cosmochimica Acta*, 63, 95-112.

Mysen, B.O., Virgo, D., and Scarfe, C.M. (1980) Relations between the anionic structure and viscosity of silicate melts—a Raman spectroscopic study. *American Mineralogist*, 65, 690–710.

Nagashima, S., and Katsura, T. (1973) The solubility of S in Na₂O–SiO₂ melts under various oxygen partial pressures at 1100 °C, 1250 °C, and 1300 °C. *Bulletin Chemical Society of Japan*, 46, 3099–3103.

Neuville, D.R., and Mysen, B.O. (1996) Role of the Al in the silicate network: in situ, high temperature study of glasses and melts on the join SiO₂-NaAlO₂. *Geochimica et Cosmochimica Acta*, 60, 1727–1737.

O'Neill, H.S.C., and Mavrogenes, J.A. (2002) The sulfide capacity and the sulfur content at sulphide saturation of silicate melts at 1400 °C and 1 bar. *Journal of Petrology*, 43, 1049–1087.

Oppenheimer, C., Scaillet, B., and Martin, R.S. (2011) Sulfur degassing from volcanoes: source conditions, surveillance, plume chemistry and earth system impacts. Sulfur in magmas and melts: its importance for natural and technical processes. In: Behrens, H., Webster, J.D. (Eds.), Washington, Mineralogical Society of America, *Geochemical Society Reviews in Mineralogy and Geochemistry*, 73, 363–421.

Paris, E., Giuli, G., Carroll, M.R., and Davoli, I. (2001) The valence and speciation of sulfur in glasses by X-ray absorption spectroscopy. *Canadian Mineralogist*, 39, 331–339.

Pasquarello, A., Sarnthein, J., and Car, R. (1998) Dynamic structure factor of vitreous silica from first principles: comparison to neutron-inelastic-scattering experiments. *Physical Review B*, 57, 14133–14140.

Pasquarello, A. (2001) First-principles simulation of vitreous systems. *Current Opinion in Solid State and Material Science*, 5, 503–508.

Pichavant, M., Scaillet, B., Di Carlo, I., Rotolo, S., and Métrich, N. (2006). Sulfur in hydrous, oxidized, basaltic magmas: phase equilibria and melt solubilities. Abstract AGU Spring Meeting, Baltimore.

Pownceby, M.I., and O'Neill, H.S.C. (1994) Thermodynamic data from redox reactions at high temperatures. IV. Calibration of the Re-ReO₂ oxygen buffer from EMF and NiO + Ni-Pd redox sensor measurements. *Contributions to Mineralogy and Petrology*, 118, 130-137.

Robie, R.A., and Hemingway, B.S. (1995) Thermodynamic properties of minerals and related substances at 298.15 K and 1 bar (10^5 Pascals) pressure and at higher temperatures. U.S. G.P.O.; U.S. Geological Survey, Information Services, Bulletin 2131, pp. 461.

Rossano, S., and Mysen, B.O. (2013) Raman spectroscopy of silicate glasses and melts in geological system. In J. Dubessy, M.C. Caumon, and F. Rull, Eds., Raman spectroscopy applied to Earth Sciences and Cultural Heritage, EMU Notes in Mineralogy, Eötvös University Press, Budapest, 12, 321–366.

Scaillet, B., and Macdonald, R. (2006) Experimental and thermodynamic constraints on the sulphur yield of peralkaline and metaluminous silicic flood eruptions. *Journal of Petrology*, 47 (7), 1413–1437.

Scaillet, B., and Pichavant, M. (2005) A model of sulphur solubility for hydrous mafic melts: application to the determination of magmatic fluid compositions of Italian volcanoes. *Annals of Geophysics*, 48, 671–697.

Scaillet, B., Luhr, J.F., and Carroll, M.C. (2003) Petrological and volcanological constraints on volcanic sulphur emissions to the atmosphere. *Volcanism and the Earth's atmosphere*. A. Robock and C. Oppenheimer. *Geophysical Monograph*, 139, 11–40.

Seifert, F., Mysen, B.O., and Virgo, D. (1982) 3-dimensional network structure of quenched melts (glass) in the systems $\text{SiO}_2\text{--NaAlO}_2$, $\text{SiO}_2\text{--CaAl}_2\text{O}_4$ and $\text{SiO}_2\text{--MgAl}_2\text{O}_4$. *American Mineralogist*, 67, 696–717.

Stelling, J., Behrens, H., Wilke, M., Göttlicher, J., and Chalmin-Aljanabi, E. (2011) Interaction between sulphide and H_2O in silicate melts. *Geochimica and Cosmochimica Acta*, 75, 3542–3557.

Stevenson, D.S., Johnson, C.E., Highwood, E.J., Gauci, V., Collins, W.J., and Derwent, R.G. (2003) Atmospheric impact of the 1783–1784 Laki eruption: Part I Chemistry modelling. *Atmospheric Chemistry and Physics*, 3, 487–507.

Symonds, R.B., Rose, W.I., Bluth, G.J.S., and Gerlach, T.M. (1994) Volcanic-gas studies: Methods, results and applications. In M.R. Carroll and J.R. Holloway, Eds., *Volatiles in Magmas*, Reviews in Mineralogy, Mineralogical Society of America, Chantilly, Virginia, 30, 1–66.

Thomas, R. (2000) Determination of water contents of granite melt inclusions by confocal laser Raman microprobe spectroscopy. *American Mineralogist*, 85, 868–872.

Tsujimura, T., Xue, X., Kanzaki, M., and Walter, M.J. (2004) Sulfur speciation and network structural changes in sodium silicate glasses: constraints from NMR and Raman spectroscopy. *Geochimica and Cosmochimica Acta*, 68, 5081–5101.

Vigouroux N., Wallace, P.J., and Kent, A.J.R. (2008) Volatiles in high-K magmas from the Western Trans-Mexican volcanic belt: Evidence for fluid fluxing and extreme enrichment of the mantle wedge by subduction processes. *Journal of Petrology* 49, 1589-1618.

Webster, J.D., and Botcharnikov, R.E. (2011) Distribution of sulfur between melt and fluid in S–O–H–C–Cl-bearing magmatic systems at shallow crustal pressures and temperatures. Sulfur in Magmas and Melts: Its Importance for Natural and Technical Processes: Reviews in Mineralogy & Geochemistry. *Mineralogical Soc Amer*, 73, 247–283.

Webster J.D., Sintoni M.F., and De Vivo, B. (2009) The partitioning behavior of Cl, S, and H₂O in aqueous vapor- ±saline-liquid saturated phonolitic and trachytic melts at 200 MPa. *Chemical Geology*, 263, 19-36.

White, S.N. (2009) Laser Raman spectroscopy as a technique for identification of seafloor hydrothermal and cold seep minerals. *Chemical Geology*, 259, 240–252.

Wilke, M., Jugo, P.J., Klimm, K., Susini, J., Botcharnikov, R., Kohn, S.C., and Janousch, M. (2008) The origin of S^{4+} detected in silicate glasses by XANES. *American Mineralogist*, 93, 235–240.

Wilke, M., Klimm, K., and Kohn, S.C. (2011) Spectroscopic studies on sulfur speciation in synthetic and natural glasses. In: Behrens, H., Webster, J.D. (Eds.), *Sulfur in Magmas and Melts: Its Importance for Natural and Technical Processes*. Washington, Mineralogical Society of America, Geochemical Society, *Rev. Mineral. Geochem.*, 73, 41–78.

Zajacz, Z. (2015) The effect of melt composition on the partitioning of oxidized sulfur between silicate melts and magmatic volatiles. *Geochimica and Cosmochimica Acta*, 158, 223–244.

Zajacz, Z., Halter, W., Malfait, W.J., Muntener, O., Bodnar, R.J., Bahcmann, O., Webster, J.D., Ulmer, P., Mandeville, C.W., Hirschmann, M.M., and Morizet, Y. (2005) A composition independent quantitative determination of the water content in silicate glasses and silicate melt inclusions by confocal Raman spectroscopy. *Contributions to Mineralogy and Petrology*, 150, 631–642.

Zolotov, M.Y., and Fegley, B. (1999) The oxidation state of volcanic gases and interior of Io. *Icarus*, 141, 40–52.

Figures

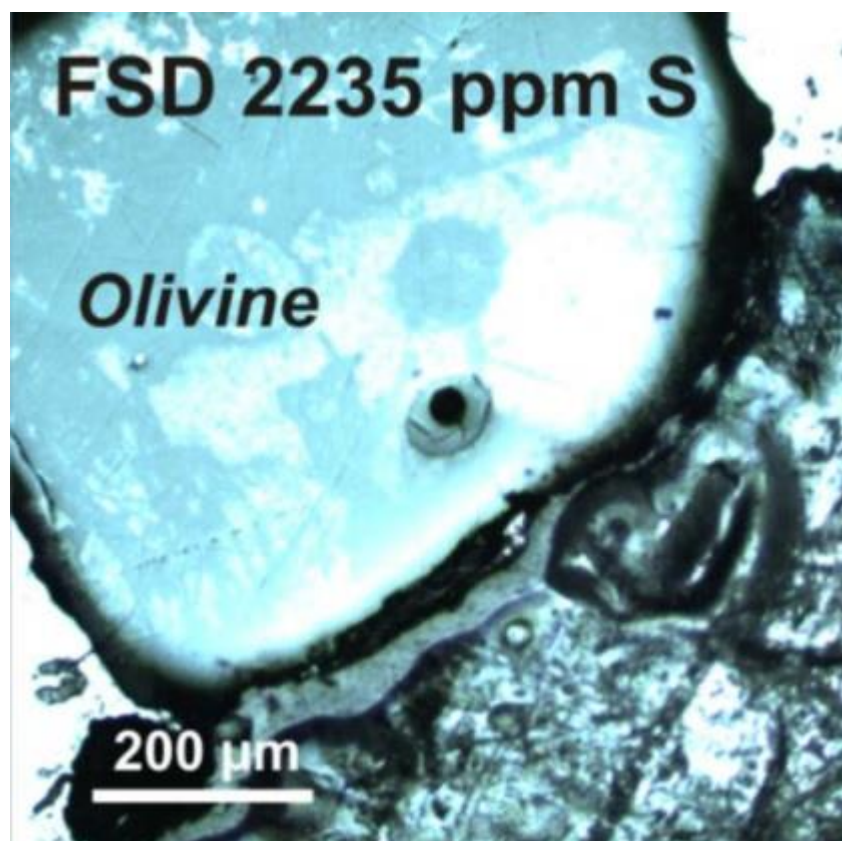


Figure 1. Microphotograph of basaltic glass inclusion hosted in olivine crystal collected from Etna lava flow. Picture was obtained from the LabRam HR 800 camera in reflective light with objective $\times 5$. The size of the glass inclusions is on the order of $50\ \mu\text{m}$. (Color online.)

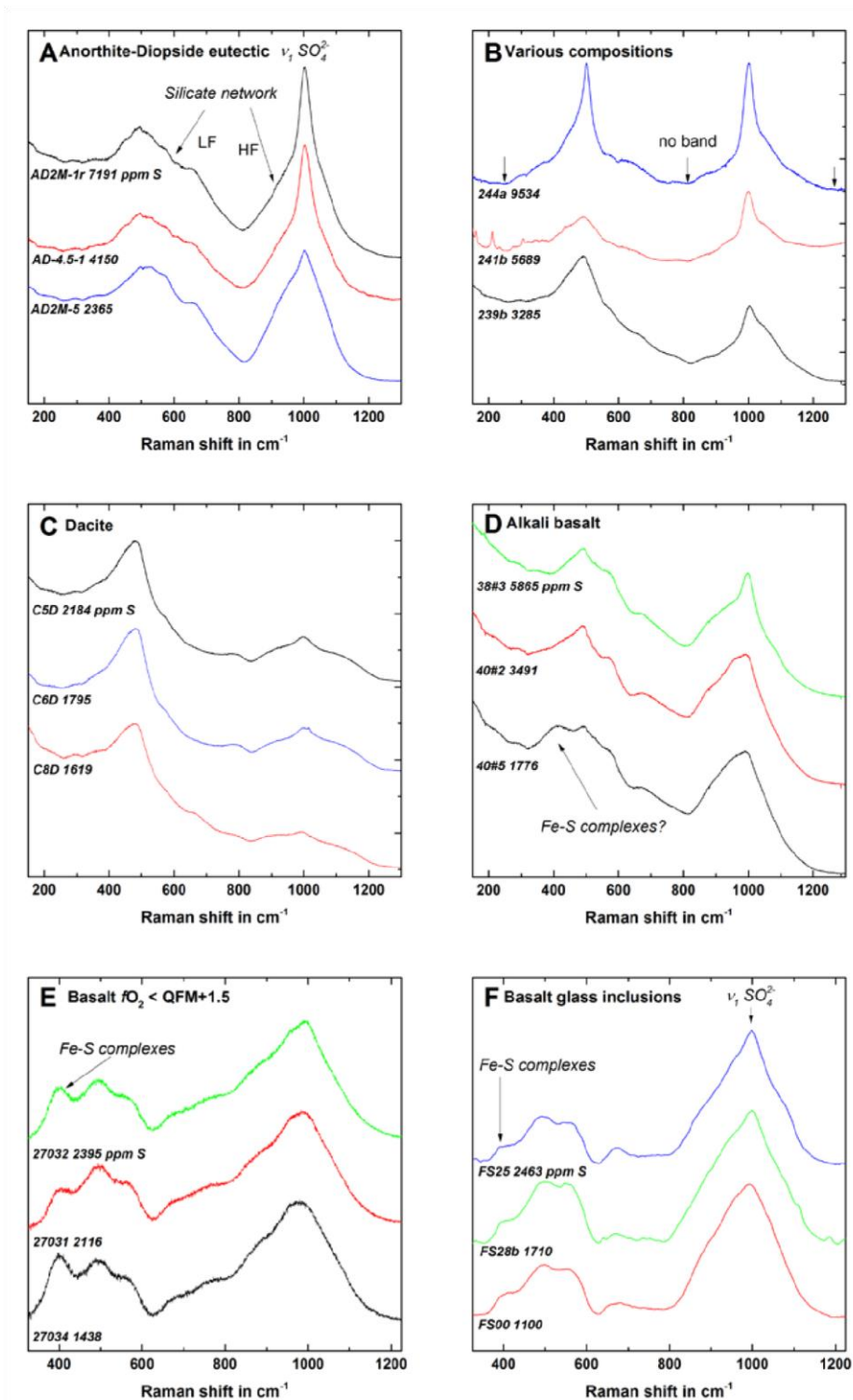


Figure 2. Raman spectra obtained on different S-bearing silicate glasses. (a) Anorthitediopside eutectic glasses from Morizet et al. (2013a, 2015a). (b) Various glass composition from Zajacz (2015). (c) Dacitic glasses from Jégo and Pichavant (2012). (d) Alkali basalt glasses from Lesne (2008) and Lesne et al. (2011). (e) Basalt glasses synthesized at $f\text{O}_2 < \text{QFM}+1.5$ from Gennaro (2017). (f) Natural basalt melt inclusions hosted in olivine crystals from Etna (Gennaro 2017). For a to d, acquisitions were conducted on the Labram 300; for e and f, acquisitions were conducted on the Labram HR 800.

The parts per million of S determined from EPMA as well as the name of the corresponding sample is reported next to each spectrum. The Raman spectrum is divided in two regions low frequency (LF) and high frequency (HF) and evidence for SO_4^{2-} species is shown by the peak at $\sim 1000 \text{ cm}^{-1}$. The band areas are shown in b. Typical third-order polynomial baseline function has been added to a and b. For glasses synthesized under moderately reducing conditions (e) and natural melt inclusions (f), the presence of S_2^{2-} species is suspected as evidenced from the prominent peak at 400 cm^{-1} . (Color online.)

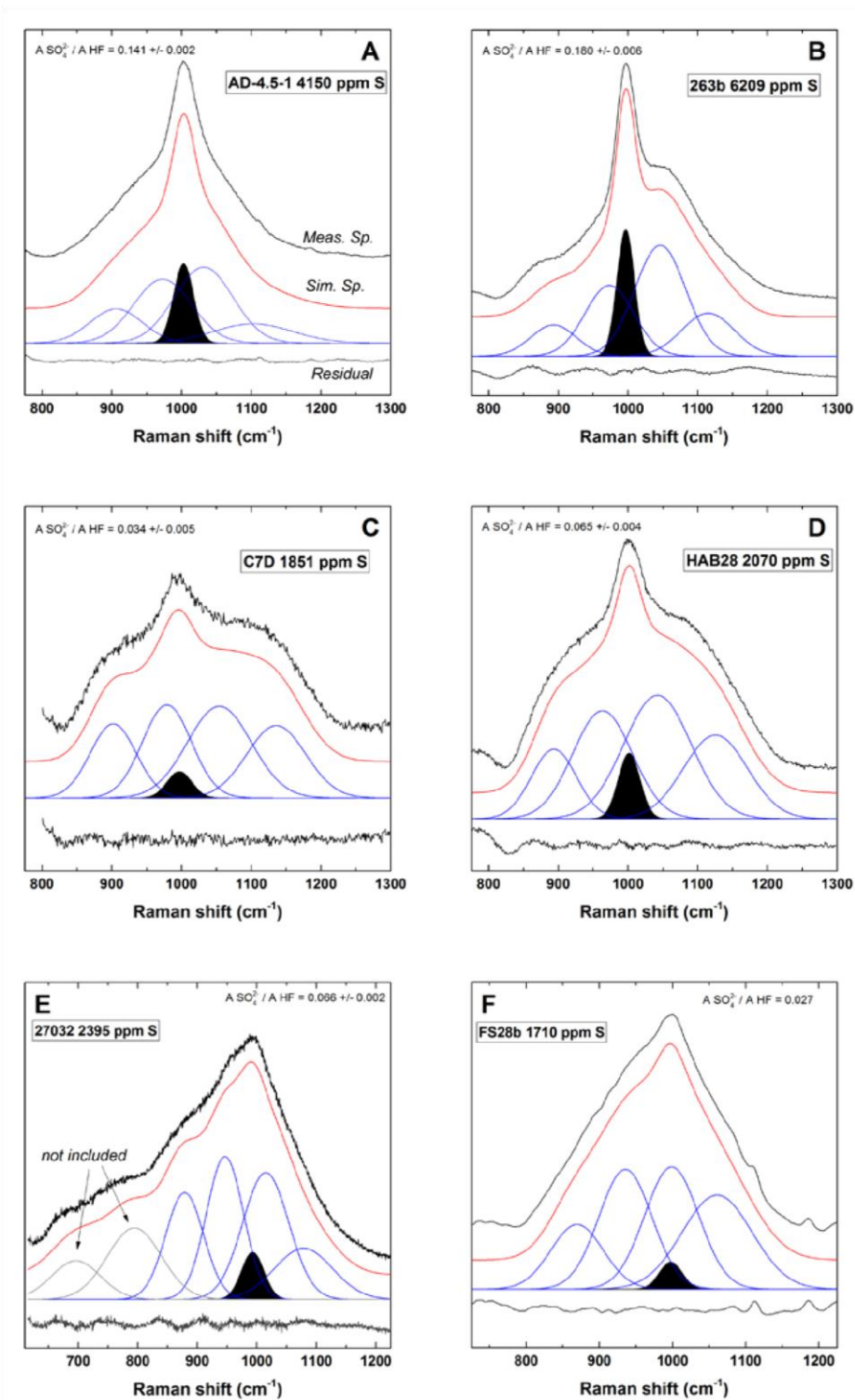


Figure 3. Typical Raman spectrum deconvolution for different silicate glasses in the HF spectral region. The entire set of deconvolution parameters is reported in Table 1 and Supplementary1 Material 1. Except for basalt glasses synthesized at $fO_2 < QFM+1.5$ (e); Raman spectra were deconvoluted with four Gaussian lines for Qn species and one Gaussian line for ν_1 SO_4^{2-} (black line). The simulated spectrum is reported underneath each spectrum. The Gaussian lines are shown as well as the residual from the simulation. The $A_{SO_4^{2-}}/A_{HF}$ ratio is reported and calculated from the determined areas of each Gaussian line. The indicated error corresponds to the standard deviation obtained on the replicated deconvolutions (see Supplementary1 material 1). (Color online.)

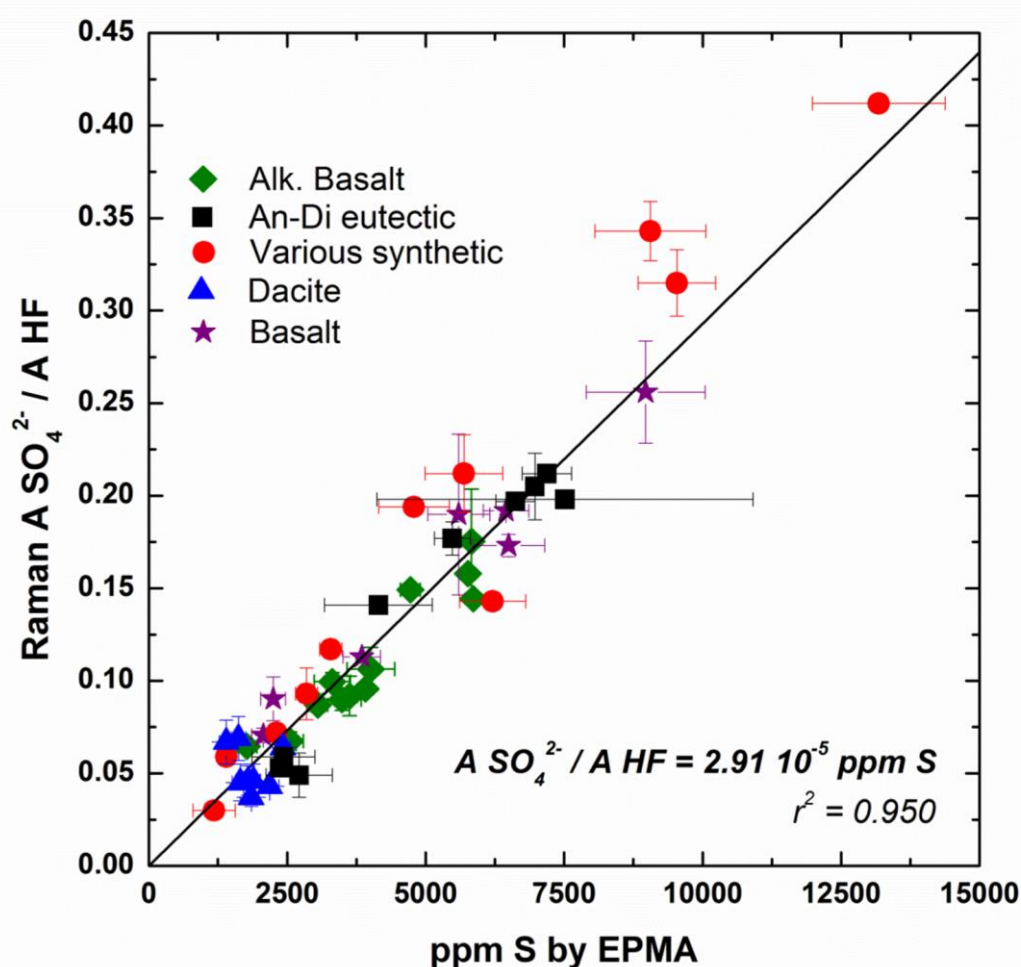


Figure 4. Raman $A_{SO_4^{2-}}/A_{HF}$ ratio determined from spectra deconvolutions as a function of parts per million of S measured by EPMA for the different investigated compositions. The $A_{SO_4^{2-}}/A_{HF}$ ratio is linearly correlated to the parts per million of S from EPMA and appears to be independent of glass composition. The linear correlation factor is reported (2.91×10^{-5}) and the r^2 representing the prediction is 0.950 based on 47 data points. Inversion to obtain the parts per million of S_{6+} from Raman calibration is provided in the text as Equation 1. (Color online.)

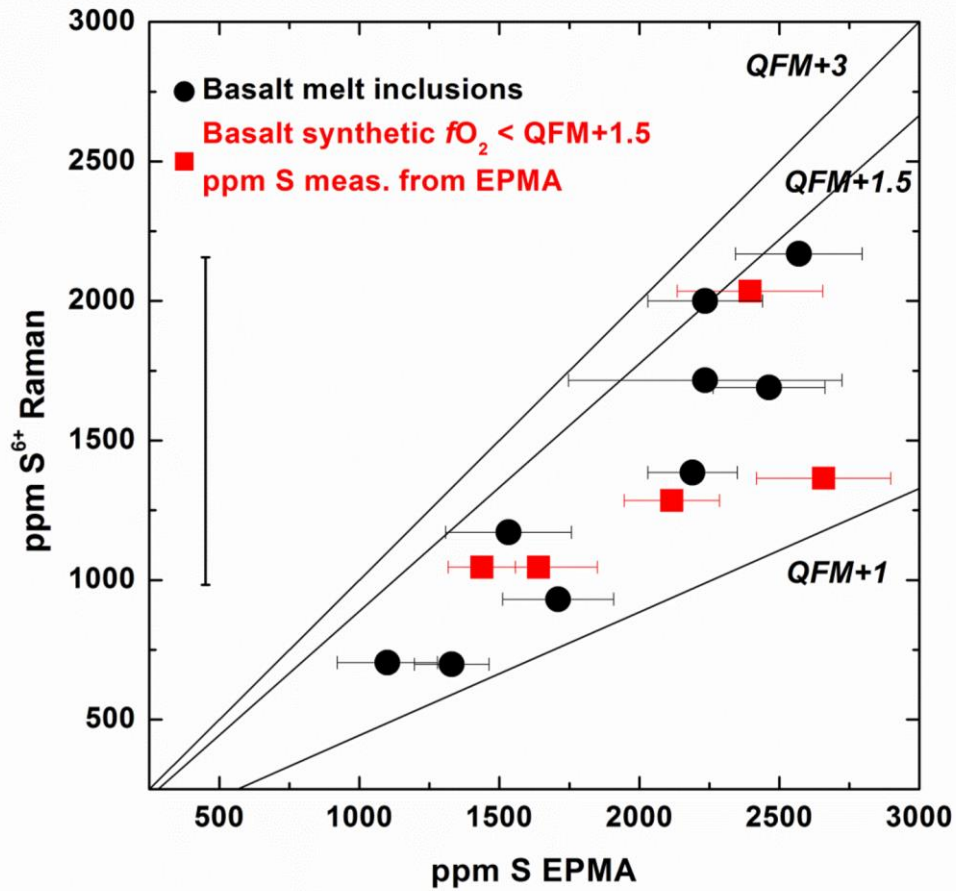


Figure 5. Parts per million of S^{6+} determined from Raman calibration as a function of parts per million of S determined from EPMA measurements from Gennaro (2017) and Iacono-Marziano et al. (2017) for basalt melt inclusions collected from Etna lava flows and basalt glasses synthesized at high pressure (80–200 MPa) and fO_2 conditions below QFM+1.5 (see Appendix 1 Table 1). Raman measurements are in favor of an unaccounted amount of S attributed to S^{2-} species. We show the calculated parts per million of S^{6+} evolution line as a function of total S content for different fO_2 (QFM+1, +1.5, and +3) from the equation of Jugo et al. (2010). (Color online.)

Table 1:

Sample	Major element chemical composition in wt. %							fO_2 ΔQFM	XS ⁶⁺	Ppm S
	SiO ₂	Al ₂ O ₃	FeO ^{tot}	MgO	CaO	Na ₂ O	K ₂ O			
Morizet et al. (2013, 2015) Anorthite – Diopside eutectic										
AD2M-5	50.1	13.0		8.5	23.1			> +1	1	2365 (138)
AD10M-5	50.2	13.3		8.7	22.8			> +1	1	5481 (324)
AD2M-1r	50.2	15.7		10.6	23.4			> +1	1	7191 (447)
AD10 na	50.2	15.7		10.6	23.4			+2.3	1	6973 (73)
AD-4.7-0.5	51.4	15.0		10.6	22.9			+2.8	1	2434 (567)
AD-4.5-1	52.2	14.8		9.3	23.5			+2.1	1	4150 (974)
AD-5-3	52.0	14.6		9.1	24.1			+1.8	1	6621 (355)
AD-5-5	53.2	15.5		8.9	22.2			+2.3	1	7519 (3397)
AD4	51.3	15.2		10.7	22.8			+2	1	2718 (598)
Jégo and Pichavant (2015) Dacite										
C6D	68.1	16.4	2.8	2.4	2.6	5.3	2.0	> +3.9	1	1795 (222)
C7D	67.7	17.2	4.2	1.7	3.4	4.6	0.7	> +3.9	1	1851 (138)
C5D	67.9	16.2	3.1	2.7	2.6	5.1	2.0	> +3.9	1	2184 (170)
C4D	67.7	16.1	3.1	2.7	3.0	5.1	1.9	> +3.9	1	2422 (146)
C3D	67.2	16.3	4.0	2.4	3.3	4.6	1.6	> +3.9	1	1651 (140)
C2D	68.0	16.6	3.6	2.3	2.6	4.7	1.7	> +3.9	1	1892 (116)
C8D	67.6	17.1	4.2	1.7	3.5	4.7	0.7	> +3.9	1	1619 (132)
C9D	67.2	17.1	4.3	1.7	3.8	4.6	0.7	> +3.9		1400 (128)
Zajacz (2015) Various compositions										
263a	52.6	14.4			16.8	5.5		> +1.8	1	13180 (481)
263b	53.7	14.6			14.4	7.9		> +1.8	1	6209 (240)
272b	53.8	18.6	4.8	0.6	1.5	7.4	5.0	> +1.8	1	2306 (61)
286a	51.3	15.1	6.3	4.1	6.8	3.2	0.8	> +1.8	1	2847 (80)
272a	53.8	15.8	6.6	4.2	6.9	4.1	1.0	> +1.8	1	1179 (152)
239a	56.2	15.6		11.0	7.4			> +1.8	1	1402 (41)
286b	51.6	17.2	4.54	0.7	1.7	6.8	4.7	> +1.8	1	4788 (256)
245a	51.9	14.6			21.8			> +1.8	1	9054 (401)

241b	53.8	14.6		2.4	18.3			> +1.8	1	5689 (280)
239b	55.2	15.2		4.8	15.8			> +1.8	1	3285 (80)
244a	53.2	14.4			18.0	3.5		> +1.8	1	9534 (280)
Pichavant et al. (XXXX) Basalt										
Ca3	51.7	17.6	6.3	7.5	10.4	2.7	0.6	+2.5	1	6500 (650)
idc10-5	52.0	17.3	7.9	5.7	9.6	2.7	2.3	+2	1	5600 (560)
HAB27	54.2	19.2	7.1	3.5	9.3	4.4	0.9	+2	1	2250 (225)
HAB28	59.8	20.3	3.0	4.1	6.9	4.0	0.9	+4	1	2070 (207)
Lesne (2008), Lesne et al. (2011) Basalt										
Run 33#2	46.2	15.8	10.3	6.3	9.7	3.4	1.9	+2.4	1	3058 (171)
Run 33#3	47.7	14.5	8.5	8.0	11.6	2.4	1.8	+2.4	1	3317 (326)
Run 38#1	46.9	13.5	8.0	6.8	12.4	1.9	9.3	+2.4	1	5764 (76)
Run 38#2	47.4	15.7	11.1	6.4	10.1	3.3	4.1	+2.4	1	5832 (96)
Run 38#3	48.1	14.1	8.8	8.3	11.9	2.2	5.6	+2.4	1	5865 (78)
Run 40#2	47.6	13.6	6.9	6.9	12.4	1.9	5.6	+2.4	1	3491 (349)
Run 40#3	48.6	13.9	7.4	6.9	12.4	1.8	7.9	+2.4	1	4013 (429)
Run 40#4	48.2	16.1	9.7	6.8	10.8	3.4	3.2	+2.4	1	2553 (241)
Run 40#5	50.1	14.8	7.6	8.5	12.5	2.2	3.4	+2.4	1	1776 (182)
Run 45#1	48.5	13.9	8.2	7.1	12.3	1.8	7.1	+2.4	1	3629 (137)
Run 45#2	48.9	16.0	8.6	6.4	10.6	3.3	4.3	+2.4	1	3915 (89)
Run 45#3	49.3	14.7	8.4	8.3	12.3	2.1	3.8	+2.4	1	4725 (176)
Gennaro (2016) Basalt moderately reduced 200 MPa, 1200°C										
27042	49.0	14.1	9.6	9.1	11.3	3.4	1.3	+1.1	0.6	1640 (210)
27031	49.4	14.4	8.6	9.1	11.7	3.3	1.3	+1.4	0.8	2116 (170)
27032	50.1	14.5	7.3	9.4	11.9	3.3	1.3	+1.4	0.8	2395 (260)
27034	50.0	14.6	7.5	9.3	11.8	3.4	1.3	+1	0.4	1438 (120)
Gennaro (2016) Basalt melt inclusions, fO2 unknown										
FS00	49.0	10.2	8.6	10.8	13.2	1.9	0.8	unknown	unknown	1100 (179)
FS3	47.2	9.54	8.55	10.48	13.40	1.70	0.75	unknown	unknown	1533 (225)
FS28a	44.3	9.32	8.42	11.49	13.36	1.56	0.65	unknown	unknown	2570 (226)
FS28b	46.0	9.46	8.12	11.07	14.01	1.58	0.78	unknown	unknown	1710 (198)
FSX	44.1	10.28	7.76	10.10	13.80	1.74	1.09	unknown	unknown	2190 (160)

FS25	n.a.	n.a.	n.a.	n.a.	n.a.	n.a.	n.a.	unknown	unknown	2463 (200)
FSB	44.0	9.20	8.08	11.27	13.28	1.43	0.87	unknown	unknown	2235 (205)
FSD	44.7	10.26	7.91	11.12	12.55	1.86	0.84	unknown	unknown	2235 (488)
SPAGNOLO	46.7	16.42	9.24	6.25	9.49	4.52	1.81	unknown	unknown	1330 (133)

